Nano Energy 53 (2018) 753–762

Contents lists available at ScienceDirect

Nano Energy

journal homepage: www.elsevier.com/locate/nanoen

Full paper

Chemomechanical interplay of layered cathode materials undergoing fast charging in lithium batteries

Sihao Xia[a,b,1], Linqin Mu[c,1], Zhengrui Xu[c], Junyang Wang[d], Chenxi Wei[b], Lei Liu[a], Piero Pianetta[b], Kejie Zhao[e], Xiqian Yu[d,*], Feng Lin[c,*], Yijin Liu[b,*]

[a] School of Electronic and Optical Engineering, Nanjing University of Science and Technology, Nanjing, Jiangsu 210094, China
[b] Stanford Synchrotron Radiation Lightsource, SLAC National Accelerator Laboratory, Menlo Park, CA 94025, USA
[c] Department of Chemistry, Virginia Tech, Blacksburg, VA 24061, USA
[d] Beijing National Laboratory for Condensed Matter Physics, Institute of Physics, CAS, Beijing 100190, China
[e] School of Mechanical Engineering, Purdue University, West Lafayette, IN 47906, USA

ARTICLE INFO

Keywords:
Cathode
Li-ion battery
Crack
Transmission X-ray microscopy
Fast charging
Chemomechanical interplay

ABSTRACT

Morphological defects contribute to chronic and acute failures of batteries. The development of these morphological defects entails the multiscale chemo-mechanical coupling associated with internal mechanical stress. The mechanical stress, caused by anisotropic structural, chemical and state of charge (SOC) heterogeneities, is released through crack formation, undermining the continuous diffusion pathways of electrons and ions and creating fresh surfaces for electrode–electrolyte side reactions. The understanding of chemomechanical interplay has remained at the descriptive level, thus, the quantification or model to fingerprint these processes is highly desired. Herein, we systematically investigate the mesoscale morphological defects within $LiNi_{0.6}Mn_{0.2}Co_{0.2}O_2$ secondary particles that have gone through fast-charging conditions. With the advanced synchrotron X-ray tomography, we nondestructively pierce the internal volume of secondary particles and quantify the morphological outcomes of the crack formation, such as porosity and internal surface area. We then develop a numerical model to predict the crack-induced diffusion deterrent of electrons and lithium ions. The mismatch between the local ionic and electronic conductivity can lead to highly heterogeneous SOC distribution in secondary particles, which exponentially deteriorates as the current density increases. Our incisive investigation of chemomechanical interplay and fast-charging can inform a knowledge base to accelerate the discovery of advanced materials that are resilient against chemomechanical failures.

1. Introduction

Alkali metal ion batteries are hierarchically structured, morphologically complex and chemically heterogeneous over a wide range of length scales. All the components in batteries synergistically execute their functionalities to perform energy storage/release. The particles of active materials are the fundamental building blocks of battery electrodes. Under practical operating conditions, the active particles often undergo many chemical and mechanical processes that deviate from what are desired. Examples of these undesired processes include but are not limited to local over-charge/discharge [1,2], surface reconstruction [3], non-uniform solid electrolyte interphase (SEI) formation [4], oxygen release [5], change of electrolyte wetting [6], deterioration of electrical contact [7], metal dissolution/precipitation [8,9] and volume expansion/contraction [10]. The interplay between these undesired side reactions at the nanoscale [11] in response to the chemomechanical events (such as buildup of mechanical stress in active particles) can lead to formation of morphological defects (e.g., microcracks). These cascade processes govern many aspects of battery performance, such as cycle life, energy density and safety.

The high voltage operation of the battery, with the potential of achieving a higher energy density, usually results in a more rapid capacity fade that hinders practical applications. Furthermore, we have witnessed increasing interest in fast-charging batteries, particularly for the applications in portable electronics and electric vehicles. Previous studies have shown that lithium storage mechanism in electrode materials could be greatly influenced by the charging rate [12]. Therefore, understanding how the chemomechanical processes of active particles

* Corresponding authors.
E-mail addresses: xyu@iphy.ac.cn (X. Yu), fenglin@vt.edu (F. Lin), liuyijin@slac.stanford.edu (Y. Liu).
[1] These authors contributed equally to this work.

https://doi.org/10.1016/j.nanoen.2018.09.051
Received 17 August 2018; Received in revised form 19 September 2018; Accepted 20 September 2018
Available online 22 September 2018

proceed as a function of charging rate can enable a knowledge base for developing batteries with improved mechanical robustness. Directly observing how electrode particles respond to different operating conditions can generate valuable insights into the formation and evolution of morphological and chemical defects. The knowledge about the origins and mechanisms of the particle degradation could critically inform the design of new battery chemistry and the synthesis of next generation battery materials aiming for improved lifetime, higher reversible capacity, and better chemomechanical robustness against undesired operating conditions, e.g. high temperature [11,13,14].

The bulk X-ray techniques, such as in-situ X-ray diffraction [15] and spectroscopy [16,17], have been widely used to study the crystal and electronic structures of active materials. Although the lattice structural information can be probed using these methods [18,19], the measured signal is averaged over a large quantity of samples and is not sensitive to the particle level heterogeneity of the battery materials [20,21]. While much attention is focused on the chemical aspects, it is well appreciated that battery failures are often associated with the mechanical processes, such as the formation of intergranular and intragranular cracks due to repeated volume changes upon Li ion extraction and insertion [22], or oxygen release at surfaces and along grain boundaries [11]. Cutting edge imaging techniques, e.g. X-ray micro/nano tomography [23–26], atomic force microscopy [27], scanning electron microscopy [28], transmission electron microscopy [29], focused ion beam and scanning electron microscopy (FIB-SEM) [30], have been used to visualize the morphological defects of the battery electrode at different length scales. The formation of cracks within and between primary particles have also been reported in electrode materials that have gone through substantially cycling [31] or thermal abused conditions [11]. The interpretation of the imaging data is, however, often descriptive and lack of a comprehensive numerical model for in-depth investigation at the mesoscale.

Herein, we systematically study the mesoscale morphological defects in the secondary particles of $LiNi_{0.6}Mn_{0.2}Co_{0.2}O_2$ (NMC) materials that have gone through different fast-charging protocols. We develop a comprehensive numerical method to model the crack induced detouring of electrons and ions in the secondary particles. Our numerical modeling shows that the degree of electrolyte infiltration into the cracks can further affect the diffusion pathway of ions, resulting in the mismatch between the local electronic and ionic conductivity within secondary particles. Such a mismatch is expected to create local SOC heterogeneity [13,32] and to accelerate the accumulation of mechanical stress that contributes to continuous crack formation. Such vicious circle is believed to be an important factor responsible for the degradation of active particles. Our results provide an unprecedented method for quantifying the evolution of chemomechanical interplay, and the knowledge obtained herein can nucleate a universal methodology for investigating chemomechanical processes in rechargeable batteries.

2. Results and discussion

2.1. Hierarchically structured Li ion battery

As discussed, the Li ion battery is hierarchically structured. In a battery, the cathode and the anode are separated by a separator and are soaked in liquid electrolyte. The cathode is made of active particles that are imbedded in a porous matrix of inactive components, e.g. carbon and binder. The structural complexity in the NMC cathode, which is the focus of this work, exist across a wide range of length scales [32] as it is illustrated in Fig. 1. The X-ray micro tomographic data of a small piece of the cathode, which has gone through extensive cycling, is shown in Fig. 1c, highlighting the large number of NMC particles that are assembled randomly. Nano-resolution X-ray transmission image of a subregion of the electrode is shown in Fig. 1d, with a few randomly selected particles imaged in the tomographic mode and presented in Fig. 1e-h. We clearly observe the mechanical disintegration of the secondary particles in Fig. 1e-h, which sets the basis for statistically viable investigation to be presented below.

2.2. Rate and particle size dependence

There is a huge parameter space for a systematic investigation of how active particles respond to practical electrochemical conditions. Some of the parameters are intrinsic to the electrode particles, e.g. the particle size and shape, whereas others are determined by specific battery operation conditions, e.g. temperature, cut-off voltage, charging rate. As the fast-charging capability emerges as an attractive goal for many battery chemistries, we first focused on evaluating the cycling rate dependence. For a systematic investigation of the morphological defects that are formed upon battery operation, we applied the transmission X-ray microscopy with nanoscale spatial resolution (~30 nm) to noninvasively reconstruct the three-dimensional (3D) morphology [33] of the NMC secondary particles. We imaged NMC electrodes that were cycled between 2.5 V and 4.5 V for 50 times under different charging-discharging rates (1 C, 2 C, 5 C and 10 C, Figs. S1-S2). Upon increasing the rate, the charge-discharge hysteresis increased and the reversible capacity decreased. The 3D mesoscale structures of these particles and the corresponding 2D virtual slices through the center of these particles are shown in Fig. 2a. In our nano-resolution X-ray imaging experiment, tens of particles from each sample were imaged in the 2D projective mode and a few (4–6) of them from each sample were more thoroughly studied in the tomography mode (see illustration in Fig. 1). One representative particle from each sample are presented in Fig. 2a. Our results suggest that the degree of cracking is positively correlated with the charging-discharging rate. The fast (dis)charging causes more irreversible particle cracking, which could be one of the major reasons for the capacity fade at high rate cycling. We point out here that a contradictory observation [29] has been reported by Xu et al. We attribute it to the difference in the electrode composition, which could be a very interesting topic for more systematic follow-up studies. To reveal the development of the morphological defects as a function of charging-discharging rate, we calculated the porosity and the specific crack surface area of the particles (Fig. 2b). There was a positive correlation between the porosity/specific crack surface area and the charging-discharging rate. Notably, a lithium ion battery is a highly complex device containing a huge number of nanoscale to mesoscale structural units (particles) due to the polycrystalline nature of cathode materials. Considering the positive correlation between the over potential and charging rate (Fig. S1), the fast charging seems to amplify the degree of variation in the chemical potential that each individual primary particle experiences. The increased heterogeneity in the distribution of chemical potential could lead to considerable local electric field and could intensify the mechanical stress that is responsible for the formation of the microcracks.

The formation of morphological defects could cause diffusion detouring of Li ions and electrons within the secondary particles. In this work, such effect is modeled using a novel numerical algorithm developed herein. Before we go into the details of this model (in the next section), we show here the quantification results (Fig. 2c and d) to complement the direct visualization (Fig. 2a) and the morphological evaluation (Fig. 2b). We introduced a parameter α to quantify the electron diffusion deterrent based on the evaluation of the probability distribution of the diffusion length increment (Supplementary Fig. S3). The crack-induced diffusion deterrent is defined as $\alpha = \int_{L_{\min}}^{L_{\max}} \frac{L \cdot P}{R} dL$, in which L is the increment of the diffusion distance, P is the relative probability and R is the radius of the particle. We note that, for the particles with similar fracture patterns, the simple summation of the increments in the diffusion length scales linearly with the particle size. In order to take out the particle size effect and to focus on the crack pattern induced diffusion deterrent, we normalize the diffusion

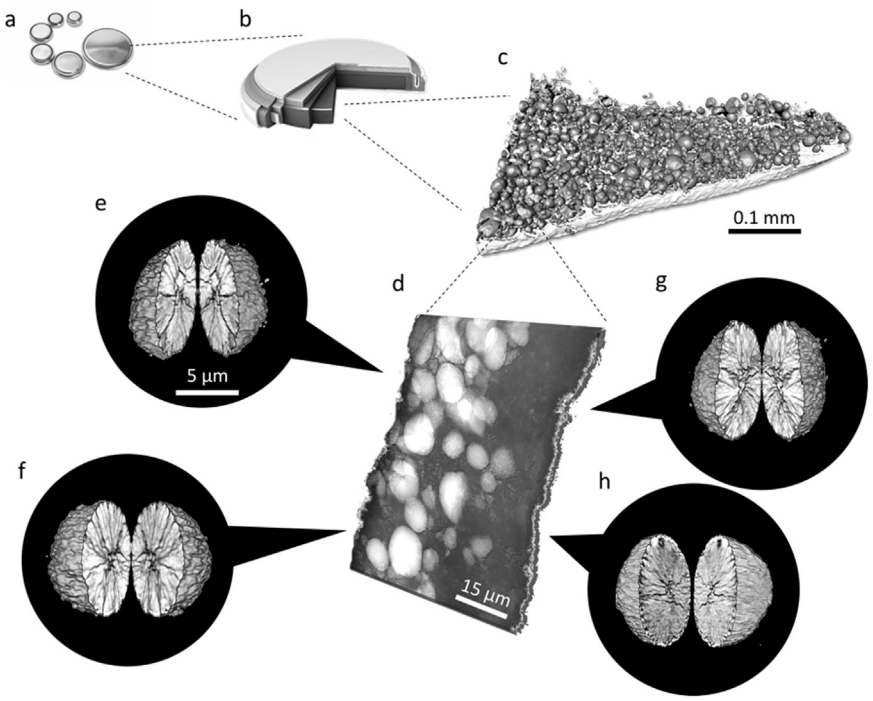

Fig. 1. X-ray micro and nano tomographic imaging of the battery electrode**.** Panels a and b illustrate the battery coin cells and their architectural structure. Panel c is the X-ray micro CT data of a small piece of cathode electrode. Panel d is the nano-resolution transmission X-ray microscopic mosaic image of a selected region on the electrode. Panels e-h are X-ray nano CT data of a few representative particles after fast cycling.

deterrent by the particle size before integrating over the entire particle volume. Therefore, the parameter α (as defined by the formula above) is chosen to quantify the crack pattern induced negative impact on the entire particle.

We show in Fig. 2c that the crack-induced diffusion deterrent (α) and the volume ratio of the unaffected regions change as a function of the charging-discharging rate. The α and the total volume of unaffected regions are inversely correlated. It is useful to understand the rearrangements of the spatial distribution of the unaffected regions within the secondary particles. We, therefore, show in Fig. 2d the depth profiles of the spatial distribution of the unaffected regions. Most of the unaffected voxels were located close to the particle surface, which was attributed to the radial distribution of cracks (Fig. 2a). The amount of internal unaffected voxels decreases rapidly as the charging-discharging rate is increased. Our observation suggests that the high rate cycling alters the diffusion kinetics of charge carriers within the secondary particles through affecting the development of the morphological defects. We note here that, in this work, the “charge carriers” refers to the electrons and the Li ions as they carry negative and positive charge, respectively, and are shuttled back and forth between the cathode and the anode of the battery. Next, we conducted a systematic analysis of the crack formation as a function of particle size. The particle size positively correlates with the degree of cracking (Fig. 3), indicating that the smaller particles are generally more robust against the formation of morphological defects under the present experimental condition. Nevertheless, in real-life batteries there are many practical limitations of small particles, such as inferior packing density [34] and accelerated cathode–electrolyte interfacial degradation [35].

2.3. *Fractures induced detouring of the electron and ion diffusion in solid state*

Upon cycling of the battery, the lattice structure of NMC experiences anisotropic expansion and contraction [36]. In additional to such anisotropic lattice evolution, the state of charge (SOC) heterogeneity is also developed within the particles [37,38]. These effects collectively build up the mechanical stress, which is ultimately released by cracking of the particles [39,40]. Such effect is evidenced by the SEM images of the particles before and after electrochemical cycling (Supplementary Fig. S4). The crack formation, in turn, can deter the diffusion of the charge carriers within the secondary particle. For simplicity, the electrolyte infiltration is not considered in this section but will be introduced later. We would emphasize here that, although the 2D SEM images could already be used to visually and qualitatively assess the degree of structural disintegration of the particles, the 3D X-ray tomographic data could facilitate more sophisticated mesoscale modeling, which will lead to more comprehensive understanding of the chemomechanical interplay at the nanoscale to the mesoscale and will be presented below. The destructive FIB-SEM technique could also be used to obtain the 3D morphology of the particle [41] with very good spatial resolution, but it is relatively more time consuming. We would also point out here that the numerical model developed herein is readily applicable to the FIB-SEM tomographic data as well.

The reconstructed 3D volume of a selected NMC particle is shown in Fig. 4a, revealing a well interconnected crack network within the secondary particle, which lay the basis for our numerical model to be presented below. Prior to the crack formation (see pristine particle structure in Figs. 2a and S4b), the geometrically optimal diffusion pathway of charge carriers from a certain voxel (a volume unit at $30 \times 30 \times 30\,nm^3$) within the 3D volume points straightly towards the particle surface (the green arrows in Fig. 4a). Once the cracks form, they act as physical barriers that force the charge carriers to detour through alternative pathways (red arrows in Fig. 4a). Charge carriers from different regions are affected differently depending on the texture and the relative location of the morphological defects. The degree of electrolyte infiltration is a critical factor that dramatically affects the diffusion pathway of the Li ion, which will be discussed later in this manuscript.

Based on this concept, we developed a numerical algorithm that solves the classic 3D maze problem. Starting at any given voxel within the 3D volume of the particle, our algorithm searches for the geometrically optimal pathway that reaches to the particle surface with the constrains set by the physical barriers, i.e. cracks. This calculation is repeated for every single voxel within the 3D volume of the secondary particle. The corresponding length of the optimal pathway is recorded and visualized (Fig. 4b and c) for a selected particle before and after crack formation, respectively. With or without cracks, the center of the particle generally has a longer diffusion length comparing to that of the

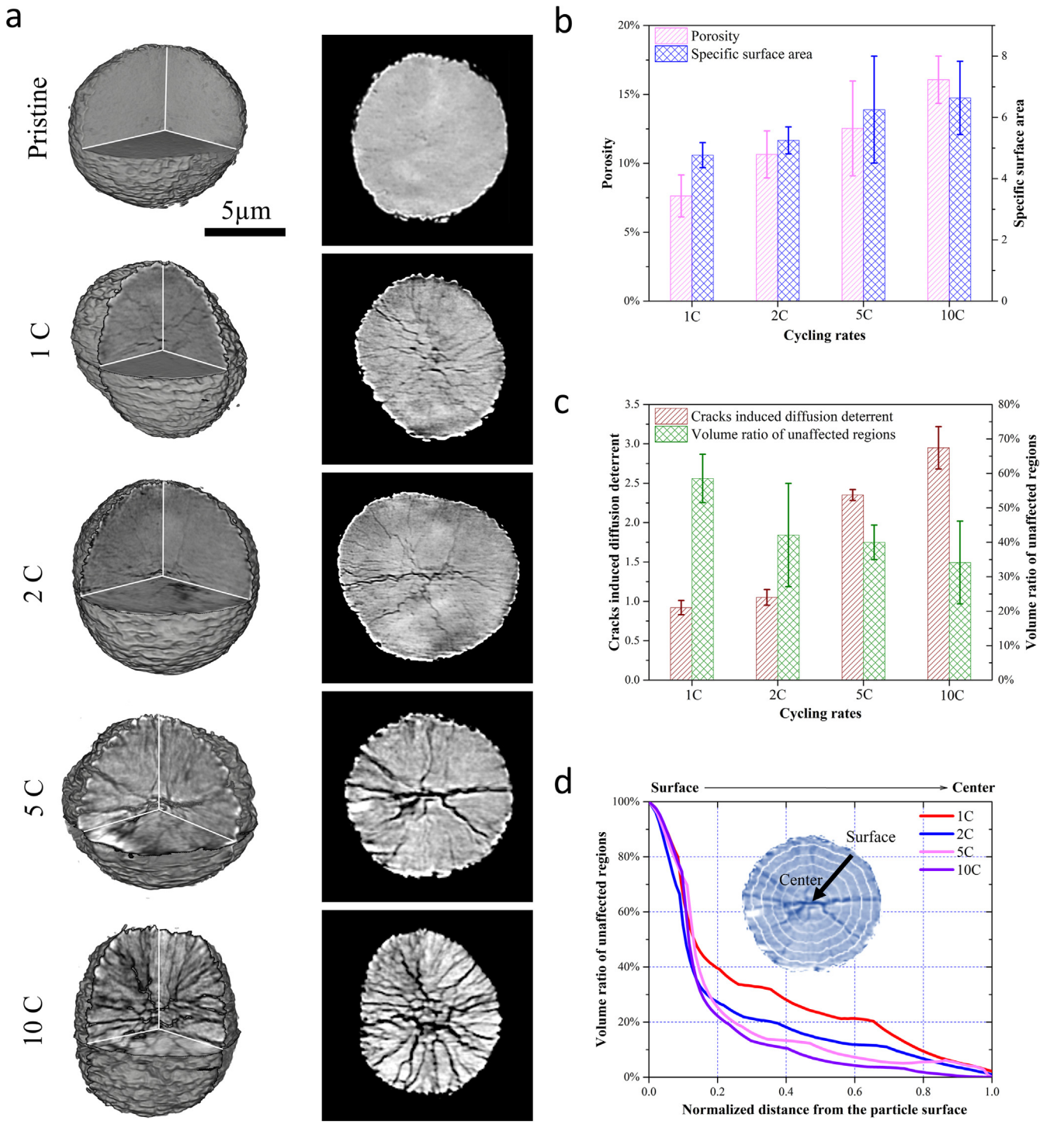

Fig. 2. Visualization and quantification of the NMC particles that were cycled for 50 times under different charging-discharging rates. (a) The 3D rendering of the particles at the pristine state and after 50 cycles at 1 C, 2 C, 5 C and 10 C. The 2D virtual slices through the centers of the particles are also shown in panel (a). (b) Quantification of the porosity and the specific crack surface area. (c) Quantification of the crack induced diffusion deterrent and the unaffected regions. (d) The depth profile of the spatial distribution of the unaffected regions.

regions near the particle surface. Subsequently, we investigate the 3D distribution of crack-induced increment in the diffusion length (Fig. 4d). As indicated by the corresponding color bars in Fig. 4, the relative increment of the diffusion length is at a level of ~10%. Affected regions in Fig. 4d are randomly distributed over the particle, highlighting the complexity of crack-induced detouring of the diffusion of charge carriers.

2.4. Electrolyte infiltration effect

In an operating Li ion battery cell, the electrode is soaked in liquid electrolyte, which possesses good ionic conductivity. The electrolyte can infiltrate into the newly developed cracks, forming new electrochemically active interfaces. The electrolyte is insulating to the electrons. As a result, the electrolyte wetting effect changes the ion diffusion pathways but does not affect the electron diffusion kinetics,

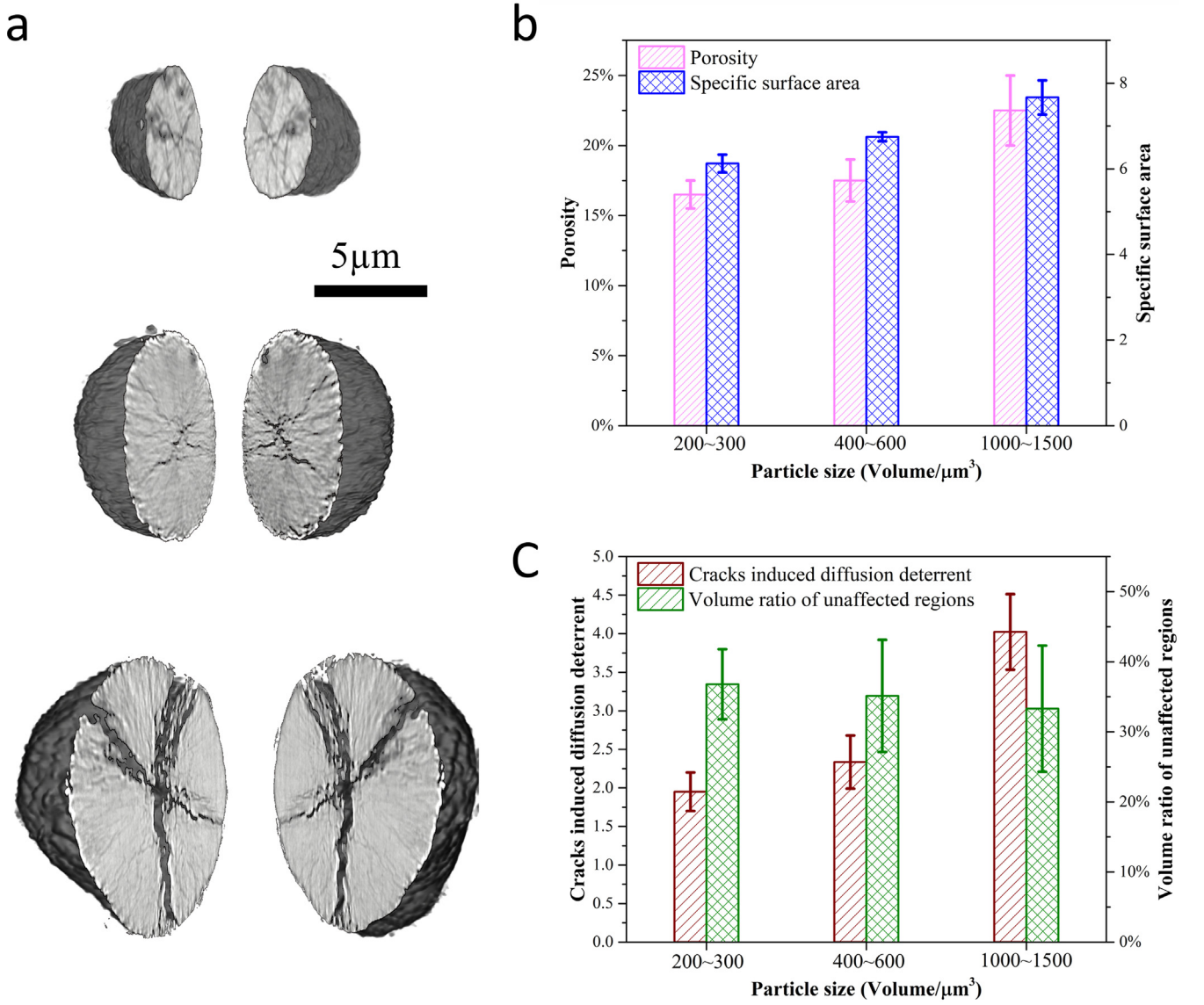

Fig. 3. Visualization and quantification of the NMC particles of different sizes. All the particles in (a) were cycled at 10 C for 50 times. (b) Quantification of the porosity and the specific crack surface area. (c) Quantification of the crack induced diffusion deterrent and the unaffected regions.

leading to a mismatch between the local ionic and electronic conductivity over the particle.

Here we include the simulation of electrolyte infiltration in our numerical model. For simplicity in the presentation of the concept, we first show in Fig. 5a and b the diffusion detouring based on a 2D slice through the center of a particle. Further statistical quantification is, however, calculated using the 3D data to reveal the real rearrangement of the electronic and ion diffusion pathways in 3D. As shown in Fig. 5a, we tune the degree of electrolyte infiltration into the cracked particle. The green arrows in Fig. 5a indicate the geometrically optimal diffusion pathways of the charge carriers prior to the particle cracking. The formation of the cracks adds additional constrains to the electron diffusion and forces the electron to detour via an alternative pathway (the red arrows), which is independent of the degree of electrolyte infiltration. The diffusion pathway of Li ions (the blue arrows) is, however, strongly affected by the electrolyte infiltration, which generally reduces the length of the geometrically optimal pathway for the Li ion. The difference between the length of the red arrows and the corresponding blue ones serves as a qualitative measurement of the mismatch between the local electronic and ionic conductivity caused by the crack formation and electrolyte infiltration. We note here that the intrinsic diffusion resistance in the layered NMC lattice structure could be different for Li ion and the electron. Although such difference is not considered here, we could effectively take it into consideration by weighting the diffusion length of the Li ion and the electron differently in our model when the intrinsic diffusion resistance is experimentally available. The spatial distribution of such mismatch over the central slice of the particle is shown in Fig. 5b, highlighting the severe mismatch that is developed as the electrolyte infiltrates towards the center of the particle through cracks. Fig. 5c shows the probability distribution of the increment of the Li ion diffusion length caused by cracks, which changes as a function of the electrolyte infiltration depth. We clearly observed that the peak shifts towards the negative direction, suggesting the reduction of the Li ion diffusion length upon electrolyte infiltration. Although it seems to favor the Li ion diffusion, the contribution of cracked particles in the cell-level electrochemical reaction is reduced. This is because the crack-induced electron diffusion deterrent becomes the dominating factor in this scenario. Moreover, the mismatch between the local electronic and ionic conductivity is rapidly developed upon electrolyte wetting as it is shown in Fig. 5d. This mismatch enhances the SOC heterogeneity and can potentially accelerate the development of more morphological defects.

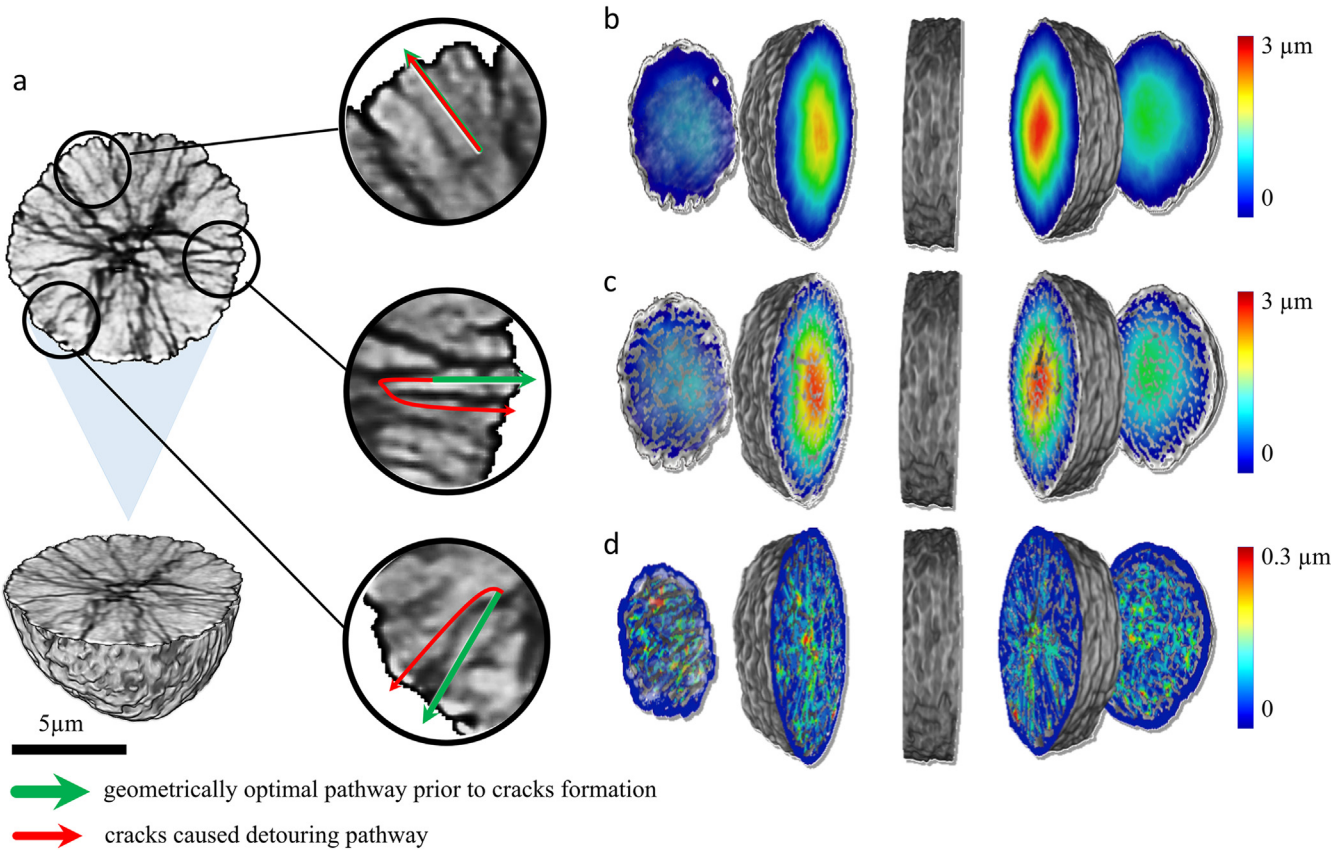

Fig. 4. The crack induced detouring of the diffusion pathways in solid state. (a) 3D rendering of the nanoscale tomographic data over a selected particle that has been cycled extensively. The morphological defects caused charge carriers detouring are shown in the insets of panel (a) schematically. The green and the red arrows are the geometrically optimal pathways before and after the crack formation, respectively. (b) Three-dimensional visualization of the geometrically optimal diffusion length over every single voxel within a pristine particle. (c) The corresponding distribution of the shortest diffusion length in the same particle that is affected by the cracks. (d) The crack formation caused increment in the diffusion length in the particle. The scale bar in panel (a) is 5 μm. (For interpretation of the references to color in this figure legend, the reader is referred to the web version of this article).

2.5. The traffic of the charge carriers on the particle surface

As discussed above, the formation of the morphological defects can cause detouring of the charge carriers within the NMC secondary particle. The crack formation can induce the increment of the diffusion length and the electrolyte infiltration into the cracks can cause mismatch between the local electronic and ionic conductivity. Here we propose that the change in the traffic load of charge carriers (electron/ion current density) over the particle surface is another important mechanism that can lead to degradation of secondary particles. In the following, we choose to evaluate the traffic load of electrons over the particle surface. We expect that the same methodology is generally applicable to quantify the traffic load of Li ions.

Based on our model, the geometrically optimal diffusion pathways (with the constrains set by the morphological defects) of every single voxel within the 3D volume of the particle can be determined using the 3D-maze-solving algorithm developed in this work. When charging an active particle, the electrons from the bulk of the particle migrate towards the particle surface where charge transfer between the particle and the surrounding environment happens. From the geometrical perspective, different surface voxels of the particle are responsible for different sub-volume within the particle. The morphological defects that are developed upon cycling of the battery, however, causes rearrangement of the diffusion pathways and, subsequently, reassigns the internal voxels to different surface voxels.

We present in Fig. 6a the 3D rendering of the particles (pristine, 0.1 C 1 cycle, 10 C 5 cycles, 10 C 10 cycles and 10 C 50 cycles) with their central slices highlighted to demonstrate the evolution of cracks within the particles. The distribution of the traffic load of electrons over the corresponding particle surface is shown in Fig. 6b. The red area and the blue area represent higher and lower local current density, respectively. With increasing cycle number, the heterogeneity of the local current density becomes enhanced as indicated by the increasing color heterogeneity in the maps shown in Fig. 6b. The redistribution of the local electronic current could cause rearrangement of the chemical segregation [12] and, subsequently, promote the chemical heterogeneity. We are aware that in practical electrodes the current distribution in active particles is also influenced by the surrounding environment such as carbon additives. The practical local current distribution is likely different from the “ideal” arrangement in our simulation presented in Fig. 6b due to the fact that our result is derived purely from the particle morphological perspective. However, the evolution of the particle morphological defects clearly enhances the heterogeneity of the local current distribution, which can lead to heterogeneous electrode-electrolyte interfacial reactions at the particle level [3,42].

3. Conclusion

Particle fracturing is a prevailing phenomenon across many energy devices that involve ion intercalation and phase transformation. In particular, the battery field has long viewed particle fracturing as an important contributing factor to chronic and acute battery failures. The development of these particle-level morphological defects is often initiated by the local structural distortion and SOC heterogeneity, which build up mechanical stress that is ultimately released through particle

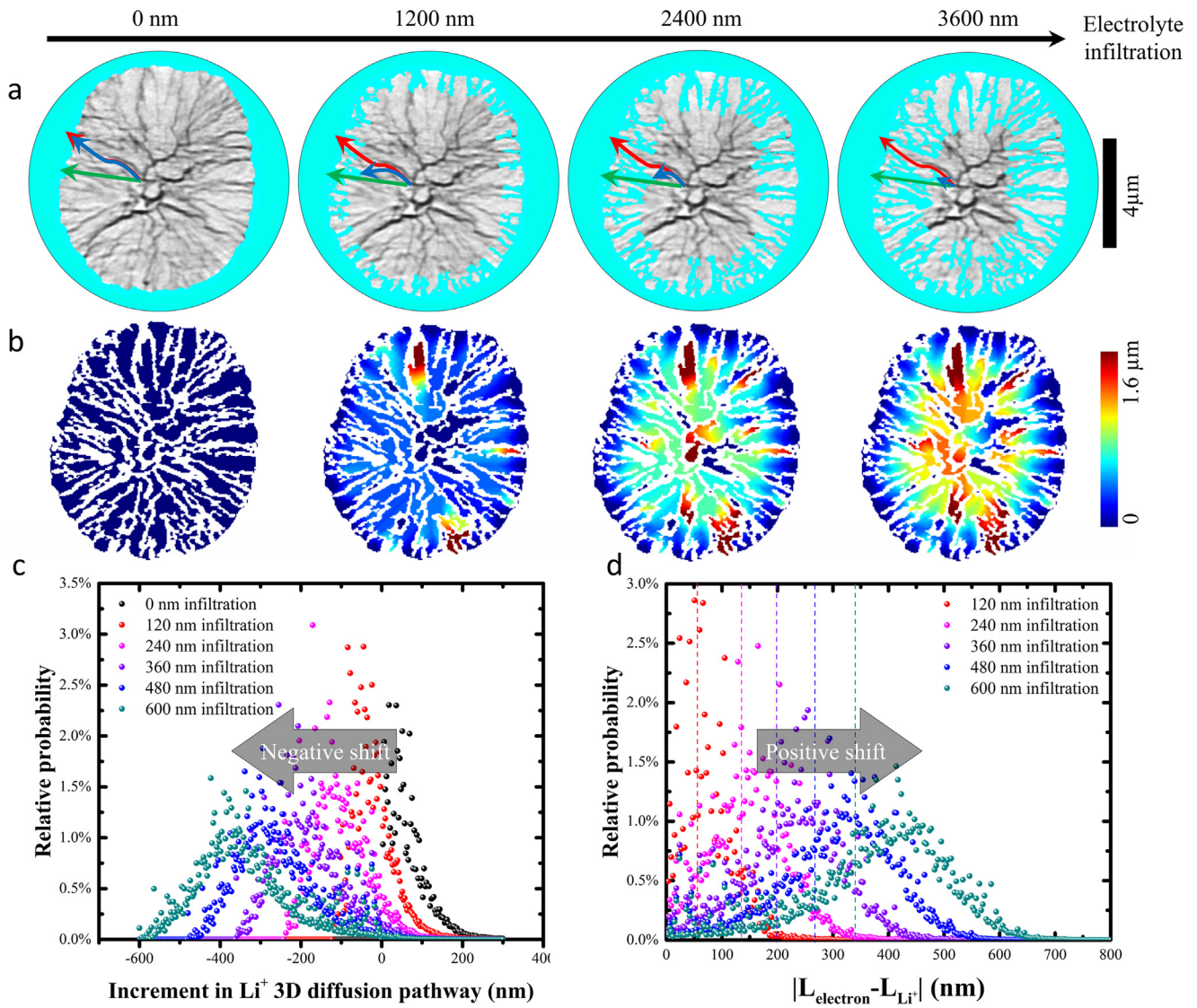

Fig. 5. Simulation of the electrolyte infiltration effect. (a) The geometrically optimal diffusion pathways of (1) both the charge carriers prior to the cracks formation (green lines), (2) the electrons after cracks formation (red lines) and (3) the Li ions after cracks formation and electrolyte infiltration (blue lines). (b) The cracking and the electrolyte infiltration induced mismatch between the local electric and ionic conductivity. (c) The evolution of the probability distribution of the cracking induced Li ion diffusion length increment upon electrolyte infiltration. (d) The evolution of the mismatch between the local electric and ionic conductivity upon electrolyte infiltration. The scale bar in panel (a) is 4 μm. (For interpretation of the references to color in this figure legend, the reader is referred to the web version of this article).

cracking. In this work, we used nano-resolution X-ray tomography, for the first time, to quantify the evolution of microcracks as a function of fast charging protocols and to establish a conceptually radical numerical method for unraveling the potential impact of microcracks on the particle-level diffusion pathways of charge carriers (see pseudo code in Fig. S6). Our study discovered that the presence of microcracks and electrolyte infiltration induced detouring of ion and electron transport in secondary particles. Microcracks significantly increased the diffusion lengths of ions and electrons. Furthermore, the electrolyte infiltration could shorten the ion diffusion length but not the electron diffusion length, resulting in a mismatch between the local electronic and ionic conductivity. Consequently, such a mismatch could lead to heterogeneous distribution of ionic and electronic traffic load over the particle surface. We suggest that such heterogeneous distribution could explain non-uniform cathode–electrolyte interphases that were widely observed in various battery materials. As it stands, our study represents an inaugural effort towards understanding and improving chemomechanical properties in polycrystalline battery materials. We also anticipate that the methodology reported herein will have a far-reaching impact on how the battery field can investigate the chemomechanical interplay of battery materials in beyond Li-ion chemistries. Future work that combines the in-situ and/or in-operando observations using multiple X-ray imaging modalities, which have been demonstrated in many case studies [26], with our numerical model could offer even more valuable insights that is relevant to the particles' dynamic response to the fast charging conditions.

4. Methods

The NMC materials were obtained from Argonne's Cell Analysis, Modeling, and Prototyping (CAMP) Facility. The composite cathodes were prepared by spreading the slurry (N-Methyl-2-pyrrolidone as the solvent) with active materials (90 wt%), acetylene carbon (5 wt%) and PVDF (5 wt%) as the binder and casting them on carbon-coated aluminum foils. The electrodes were then dried overnight at 120 °C in a vacuum oven and transferred into a Ar filled glove box for future use.

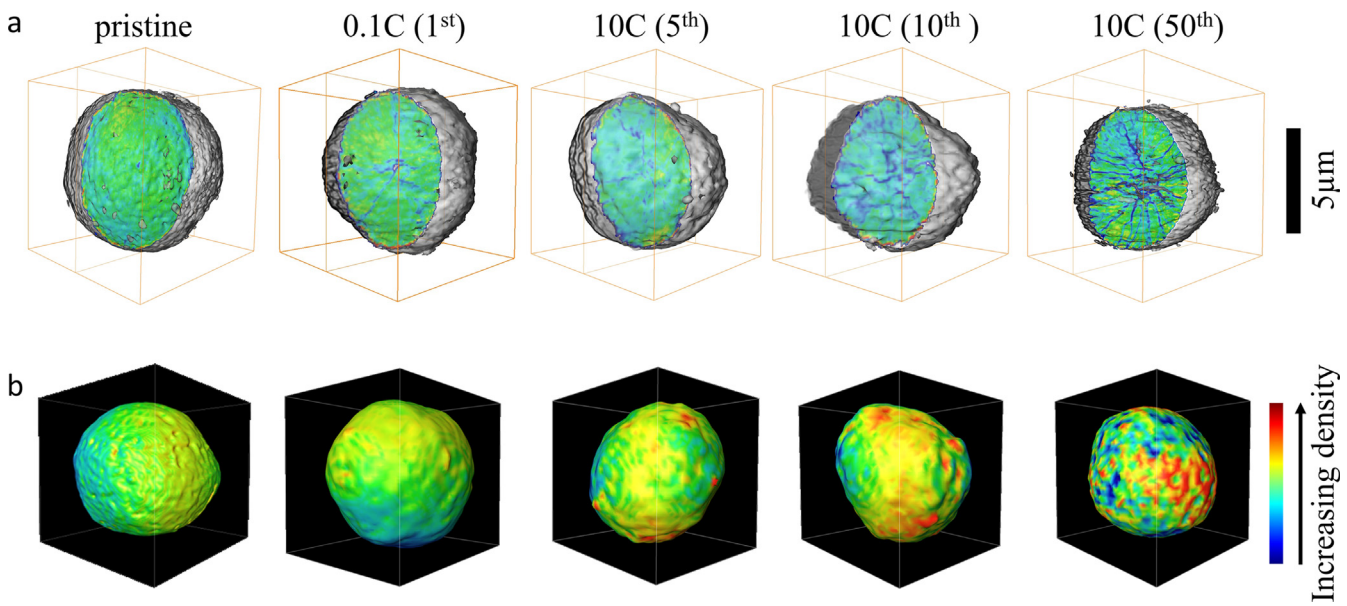

Fig. 6. Traffic map for electrons over the surface of the particles that have gone different cycling history. (a) 3D rendering of the particles of different cycling history with their central slices highlighted to illustrate the development of the morphological defects. (b) the traffic load of electrons over the corresponding particle surface. The scale bar in panel (a) is 5 μm. (For interpretation of the references to color in this figure, the reader is referred to the web version of this article).

The active mass loadings for the electrodes were 4.5 mg/cm^2. CR2032 coin cells were assembled in a Ar-filled glovebox (O_2 < 0.5 ppm, H_2O < 0.5 ppm) using the composite cathode, lithium foil (MTI) as the anode, Whatman glass fiber (1827–047 934-AH) as the separator and 1 M $LiPF_6$ dissolved in ethylene carbonate (EC) and ethyl methyl carbonate (EMC) with 2 wt% vinylene carbonate (VC) as the electrolyte. All coin cells were cycled with an electrochemical workstation (Wuhan Land Company) at 23 °C. 1 C was defined as fully charging a cathode in 1 h, corresponding to a specific current density of 200 mA/g. All the coin cells were cycled starting at C/10 for the initial cycle and then followed by various current rates (1 C, 2 C, 5 C, and 10 C). After the designated number of cycles, the coin cells were disassembled in the glovebox and the cathodes were collected for TXM and SEM characterization.

The nano-resolution X-ray tomography was performed using the transmission X-ray microscope installed at beamline 6-2C of the Stanford Synchrotron Radiation Lightsource of SLAC National Accelerator Laboratory. More details of this beamline can be found elsewhere [43]. We first conducted X-ray imaging of the secondary NMC particles on the cathode electrode to minimize the sample preparation steps. While the 3D morphology at the electrode level and at the secondary particle level is clearly visualized in the micro CT and the nano CT data (see Fig. 1), respectively, the high active material loading causes particle agglomeration in the cathode electrode and, subsequently, challenges in the nano CT measurement and reconstruction. To improve the nano CT imaging data quality, powder of cathode electrode was carefully peeled off from the Al current collector using a razor blade and was then collected and loaded into the quartz capillary tube for TXM measurements. We carefully controlled the secondary NMC particles loading in the quartz capillaries (100 μm in diameter and 10 μm in wall thickness) to ensure that we have the right degree of particle dispersion for the X-ray nano CT measurements. We chose to perform the tomography measurements at 8000 eV for the best efficiency of objective Fresnel zone plate. The nominal spatial resolution of the system is ~30 nm. The single exposure takes about 0.5 s and the samples were rotated by 180° within step size at 0.5°. An iterative tomographic reconstruction algorithm [44] was used to enhance the quality of the reconstruction results. The tomographic data reduction was performed using an in-house developed software package known as TXM-Wizard [45].

We evaluated the particle's morphological defect by calculating the porosity and the specific surface areas. The porosity is defined by the volume ratio of the void space within the secondary particle. The volume ratio of void space is obtained by a threshold segmentation of the 3D grayscale map of the particle. The detailed segmentation process can be seen in Fig. S5. For quantifying the porosity, the number of void voxels is calculated and, then, divided by the total number of voxels over the entire particle volume. The specific surface area is defined as $\xi = S/V$ [8], in which S is the surface area of the cracks and the V is the volume of the particle. The cracks induced diffusion deterrent is an impact degree to measure the negative effects of the cracks, which is associated with the increment of diffusion pathway and the particle size. The quantification of the diffusion deterrent is achieved through the 3D maze solving algorithm, which is described in details in the Supplementary Fig. S6. We use the volume ratio of unaffected regions to describe the volume ratio of voxels, whose diffusion pathway is not affected by the cracks. These voxels are of small value in the diffusion deterrent maps. The surface traffic load of electrons is used to describe the local current density over the surface of the particle. During the charging or discharging process of the battery, the reactions within the particle are accompanied by the electrons exchange between particle and external system. For a certain pixel on the particle surface, its local current density is determined by the numbers of voxels inside the particle, whose geometrical optimal diffusion pathway ends at this surface point.

Based on the 3D mesoscale structure of the NMC secondary particles reconstructed from the tomographic data, we developed a numerical algorithm to evaluate the shortest diffusion length from every single voxel within the particle to the particle surface. Firstly, we identify the outer surface of the particle, where the charge transfer between the particle and the external system happens. We assign value 2 to these surface pixels. Within the secondary particle, the voxels of the solid phase and the crack are segmented and labeled using the value 1 and −1, respectively (see Fig. S5 for the segmentation of the TXM data). Then, for all solid phase voxels adjacent to the current front, which is the original surface in the very first iteration, their value is reassigned unless their original value is smaller than calculated value, which will be elaborated next. If the voxel is vertically adjacent to the current front, then the value of this voxel is assigned as $x + 1$, where x is the value of the voxels in the current front; if the point is 2D diagonal

adjacent to the current front, then the value of this voxel is assigned as $x + \sqrt{2}$; if the point is 3D diagonal adjacent to the current front, then the value of this voxel is assigned as $x + \sqrt{3}$. After this, the current front moves one step forward and the iteration continues. Through this method, we generate a 3D matrix with the value of each voxel representing the corresponding shortest distance from the voxel to the particle surface.

The FIB-SEM measurement of the NMC electrode and particle was conducted using FEI Helios 600i. The acceleration voltage was set to 30 kV and the beam current was at 0.4 nA.

Acknowledgements

The work at IOP was supported by funding from National Key R&D Program of China (Grant no. 2017YFB0102004) and National Natural Science Foundation of China (Grant no. 51822211). F.L. and K.Z. acknowledge support from the National Science Foundation under Grants no. DMR-1832613 and DMR-1832707, respectively. The work at Virginia Tech was supported by the Department of Chemistry Startup at Virginia Tech and ORAU Ralph E. Powe Junior Faculty Enhancement Award. The NMC electrodes were produced at the U.S. Department of Energy's (DOE) CAMP (Cell Analysis, Modeling and Prototyping) Facility, Argonne National Laboratory. The CAMP Facility is fully supported by the DOE Vehicle Technologies Program (VTP) within the core funding of the Applied Battery Research (ABR) for Transportation Program. Use of the Stanford Synchrotron Radiation Lightsource, SLAC National Accelerator Laboratory, is supported by the U.S. Department of Energy, Office of Science, Office of Basic Energy Sciences under Contract no. DE-AC02-76SF00515. The engineering support from D. Van Campen, D. Day and V. Borzenets for the TXM experiment at beamline 6-2C of SSRL is gratefully acknowledged. S. Xia and W. Chen were supported by the China Scholarship Council for their study at the SLAC National Accelerator Laboratory.

Author contributions

Y. Liu, F. Lin and X. Yu designed the project. S. Xia, L. Mu, C. Wei, J. Wang, X. Yu, F. Lin, Y. Liu performed the experiments. S. Xia, X. Yu, F. Lin and Y. Liu analyzed the data. Z. Xu, L. Liu, P. Pianetta and K. Zhao contributed to the interpretation of the tomographic and electrochemical data. S. Xia, X. Yu, F. Lin and Y. Liu prepared the manuscript with critical inputs from all the authors.

Competing interests

The authors declare no competing financial interest.

Appendix A. Supporting information

Supplementary data associated with this article can be found in the online version at doi:10.1016/j.nanoen.2018.09.051.

References

[1] T. Ohsaki, T. Kishi, T. Kuboki, N. Takami, N. Shimura, Y. Sato, M. Sekino, A. Satoh, Overcharge reaction of lithium-ion batteries, J. Power Sources 146 (2005) 97–100.
[2] J. Nelson Weker, A.M. Wise, K. Lim, B. Shyam, M.F. Toney, Operando spectroscopic microscopy of $LiCoO_2$ cathodes outside standard operating potentials, Electrochimica Acta 247 (2017) 977–982.
[3] F. Lin, I.M. Markus, D. Nordlund, T.-C. Weng, M.D. Asta, H.L. Xin, M.M. Doeff, Surface reconstruction and chemical evolution of stoichiometric layered cathode materials for lithium-ion batteries, Nat. Commun. 5 (2014) 3529.
[4] M. Nie, D. Chalasani, D.P. Abraham, Y. Chen, A. Bose, B.L. Lucht, Lithium ion battery graphite solid electrolyte interphase revealed by microscopy and spectroscopy, J. Phys. Chem. 117 (2013) 1257–1267.
[5] E. Hu, S.-M. Bak, Y. Liu, J. Liu, X. Yu, Y.-N. Zhou, J. Zhou, P. Khalifah, K. Ariyoshi, K.-W. Nam, X.-Q. Yang, Utilizing environmental friendly iron as a substitution element in spinel structured cathode materials for safer high energy lithium-ion batteries, Adv. Energy Mater. 6 (2016) 1501662.
[6] M.-S. Wu, T.-L. Liao, Y.-Y. Wang, C.-C. Wan, Review in applied electrochemistry. Number 54 recent developments in polymer electrolyte fuel cell electrodes, J. Appl. Electrochem. 34 (2004) 797–805.
[7] J.N. Weker, N. Liu, S. Misra, J.C. Andrews, Y. Cui, M.F. Toney, In situ nanotomography and operando transmission X-ray microscopy of micron-sized Ge particles, Energy Environ. Sci. 7 (2014) 2771–2777.
[8] F. Yang, Y. Liu, S.K. Martha, Z. Wu, J.C. Andrews, G.E. Ice, P. Pianetta, J. Nanda, Nanoscale morphological and chemical changes of high voltage lithium–manganese rich NMC composite cathodes with cycling, Nano Lett. 14 (2014) 4334–4341.
[9] E. Billy, M. Jouli´e, R. Laucournet, A. Boulineau, E. De Vito, D. Meyer, Dissolution mechanisms of $LiNi_{1/3}Mn_{1/3}Co_{1/3}O_2$ positive electrode material from lithium-ion batteries in acid solution, ACS Appl. Mater. Interfaces 10 (2018) 16424–16435.
[10] T.R. Garrick, Y. Dai, K. Higa, V. Srinivasan, J.W. Weidner, Modeling battery performance due to intercalation driven volume change in porous electrodes, ECS Trans. 72 (2016) 11–31.
[11] L. Mu, R. Lin, R. Xu, L. Han, S. Xia, D. Sokaras, J.D. Steiner, T.-C. Weng, D. Nordlund, M.M. Doeff, Y. Liu, K. Zhao, H.L. Xin, F. Lin, Oxygen release induced chemomechanical breakdown of layered cathode materials, Nano Lett. 18 (2018) 3241–3249.
[12] Y. Xu, E. Hu, K. Zhang, X. Wang, V. Borzenets, Z. Sun, P. Pianetta, X. Yu, Y. Liu, X.-Q. Yang, H. Li, In situ visualization of state-of-charge heterogeneity within a $LiCoO_2$ particle that evolves upon cycling at different rates, ACS Energy Lett. 2 (2017) 1240–1245.
[13] L. Mu, Q. Yuan, C. Tian, C. Wei, K. Zhang, J. Liu, P. Pianetta, M.M. Doeff, Y. Liu, F. Lin, Propagation topography of redox phase transformations in heterogeneous layered oxide cathode materials, Nat. Commun. 9 (2018), https://doi.org/10.1038/s41467-018-05172-x.
[14] P. Yan, J. Zheng, T. Chen, L. Luo, Y. Jiang, K. Wang, M. Sui, J.-G. Zhang, S. Zhang, C. Wang, Coupling of electrochemically triggered thermal and mechanical effects to aggravate failure in a layered cathode, Nat. Commun. 9 (2018) 2437.
[15] P. Shearing, Y. Wu, S.J. Harris, N. Brandon, In situ X-ray spectroscopy and imaging of battery materials, Electrochem. Soc. Interface 20 (2011) 43.
[16] M. Morcrette, Y. Chabre, G. Vaughan, G. Amatucci, J.-B. Leriche, S. Patoux, C. Masquelier, J.M. Tarascon, In situ X-ray diffraction techniques as a powerful tool to study battery electrode materials, Electrochim. Acta 47 (2002) 3137–3149.
[17] M. Balasubramanian, X. Sun, X.Q. Yang, J. McBreen, In situ X-ray diffraction and X-ray absorption studies of high-rate lithium-ion batteries, J. Power Sources 92 (2001) 1–8.
[18] B. Song, S.J. Day, T. Sui, L. Lu, C.C. Tang, A.M. Korsunsky, Mitigated phase transition during first cycle of a Li-rich layered cathode studied by in operando synchrotron X-ray powder diffraction, Phys. Chem. Chem. Phys. 18 (2016) 4745–4752.
[19] F. Lin, Y. Liu, X. Yu, L. Cheng, A. Singer, O.G. Shpyrko, H.L. Xin, N. Tamura, C. Tian, T.-C. Weng, X.-Q. Yang, Y.S. Meng, D. Nordlund, W. Yang, M.M. Doeff, Synchrotron X-ray analytical techniques for studying materials electrochemistry in rechargeable batteries, Chem. Rev. 117 (2017) 13123–13186.
[20] M.M. Rahman, Y. Xu, H. Cheng, Q. Shi, R. Kou, L. Mu, Q. Liu, S. Xia, X. Xiao, C.-J. Sun, D. Sokaras, D. Nordlund, J.-C. Zheng, Y. Liu, F. Lin, Empowering multi-component cathode materials for sodium ion batteries by exploring three-dimensional compositional heterogeneities, Energy Environ. Sci. (2018), https://doi.org/10.1039/C8EE00309B.
[21] F. Lin, D. Nordlund, Y. Li, M.K. Quan, L. Cheng, T.C. Weng, Y. Liu, H.L. Xin, M.M. Doeff, Metal segregation in hierarchically structured cathode materials for high-energy lithium batteries, Nat. Energy 1 (2016) 15004.
[22] S. Zhang, Chemomechanical modeling of lithiation-induced failure in high-volume-change electrode materials for lithium ion batteries, npj Comput. Mater. 3 (2017) 7.
[23] H. Liu, M. Wolf, K. Karki, Y.-S. Yu, E.A. Stach, J. Cabana, K.W. Chapman, P.J. Chupas, Intergranular cracking as a major cause of long-term capacity fading of layered cathodes, Nano Lett. 17 (2017) 3452–3457.
[24] M. Ebner, F. Marone, M. Stampanoni, V. Wood, Visualization and quantification of electrochemical and mechanical degradation in Li ion batteries, Science 342 (2013) 716–720.
[25] L. Wang, J. Wang, F. Guo, L. Ma, Y. Ren, T. Wu, P. Zuo, G. Yin, J. Wang, Understanding the initial irreversibility of metal sulfides for sodium-ion batteries via operando techniques, Nano Energy 43 (2018) 184–191.
[26] L. Wang, J. Wang, P. Zuo, Probing battery electrochemistry with in operando synchrotron X-ray imaging techniques, Small Methods 2 (2018) 1700293.
[27] C.R. Becker, K.E. Strawhecker, Q.P. McAllister, C.A. Lundgren, In situ atomic force microscopy of lithiation and delithiation of silicon nanostructures for lithium ion batteries, ACS Nano 7 (2013) 9173–9182.
[28] R. Hausbrand, G. Cherkashinin, H. Ehrenberg, M. Gröting, K. Albe, C. Hess, W. Jaegermann, Fundamental degradation mechanisms of layered oxide Li-ion battery cathode materials: methodology, insights and novel approaches, Mater. Sci. Eng. B 192 (2015) 3–25.
[29] R. Xu, L. de Vasconcelos, J. Shi, J. Li, K. Zhao, Disintegration of meatball electrodes for LiNixMnyCozO2 cathode materials, Exp. Mech. 58 (2018) 549–559.
[30] B. Song, T. Sui, S. Ying, L. Li, L. Lu, A.M. Korsunsky, Nano-structural changes in Li-ion battery cathodes during cycling revealed by FIB-SEM serial sectioning tomography, J. Mater. Chem. A 3 (2015) 18171–18179.
[31] P. Yan, J. Zheng, M. Gu, J. Xiao, J.-G. Zhang, C.-M. Wang, Intragranular cracking as a critical barrier for high-voltage usage of layer-structured cathode for lithium-ion batteries, Nat. Commun. 8 (2017) 14101.
[32] C. Wei, S. Xia, H. Huang, Y. Mao, P. Pianetta, Y. Liu, Mesoscale battery science: the behavior of electrode particles caught on a multispectral X-ray camera, Acc. Chem. Res. (2018), https://doi.org/10.1021/acs.accounts.8b00123.
[33] F. Meirer, J. Cabana, Y. Liu, A. Mehta, J.C. Andrews, P. Pianetta, Three-dimensional imaging of chemical phase transformations at the nanoscale with full-field

transmission X-ray microscopy, J. Synchrotron Radiat. 18 (2011) 773–781.
[34] V. Dusastre, Materials for Sustainable Energy: A Collection of Peer-Reviewed Research and Review Articles from Nature Publishing Group, 18 World Scientific, 2011, pp. 773–781.
[35] J. Cabana, B.J. Kwon, L. Hu, Mechanisms of degradation and strategies for the stabilization of cathode–electrolyte interfaces in Li-ion batteries, Acc. Chem. Res. 51 (2018) 299–308.
[36] K.-W. Nam, W.-S. Yoon, H. Shin, K.Y. Chung, S. Choi, X.-Q. Yang, In situ X-ray diffraction studies of mixed $LiMn_2O_4$–$LiNi_{1/3}Co_{1/3}Mn_{1/3}O_2$ composite cathode in Li-ion cells during charge-discharge cycling, J. Power Sources 192 (2009) 652–659.
[37] W.E. Gent, Y. Li, S. Ahn, J. Lim, Y. Liu, A.M. Wise, C.B. Gopal, D.N. Mueller, R. Davis, J.N. Weker, J.-H. Park, S.-K. Doo, W.C. Chueh, Persistent state-of-charge heterogeneity in relaxed, partially charged $Li_{1-x}Ni_{1/3}Co_{1/3}Mn_{1/3}O_2$ secondary particles, Adv. Mater. 28 (2016) 6631–6638.
[38] C.S. Johnson, Charging up lithium-ion battery cathodes, Joule 2 (2018) 373–375.
[39] H.-H. Ryu, K.-J. Park, C.S. Yoon, Y.-K. Sun, Capacity fading of Ni-Rich Li$[Ni_xCo_yMn_{1-x-y}]O_2$ ($0.6 \le x \le 0.95$) cathodes for high-energy-density lithium-ion batteries: bulk or surface degradation? Chem. Mater. 30 (2018) 1155–1163.
[40] G. Sun, T. Sui, B. Song, H. Zheng, L. Lu, A.M. Korsunsky, On the fragmentation of active material secondary particles in lithium ion battery cathodes induced by charge cycling, Extrem. Mech. Lett. 9 (2016) 449–458.
[41] N. Besnard, A. Etiemble, T. Douillard, O. Dubrunfaut, P. Tran-Van, L. Gautier, S. Franger, J.-C. Badot, E. Maire, B. Lestriez, Multiscale morphological and electrical characterization of charge transport limitations to the power performance of positive electrode blends for lithium-ion batteries, Adv. Energy Mater. 7 (2017) 1602239.
[42] F. Lin, D. Nordlund, I.M. Markus, T.-C. Weng, H.L. Xin, M.M. Doeff, Profiling the nanoscale gradient in stoichiometric layered cathode particles for lithium-ion batteries, Energy Environ. Sci. 7 (2014) 3077–3085.
[43] Y. Liu, F. Meirer, J. Wang, G. Requena, P. Williams, J. Nelson, A. Mehta, J.C. Andrews, P. Pianetta, 3D elemental sensitive imaging using transmission X-ray microscopy, Anal. Bioanal. Chem. 404 (2012) 1297–1301.
[44] Y.J. Liu, P.P. Zhu, B. Chen, J. Wang, Q. Yuan, W. Huang, H. Shu, E. Li, X. Liu, K. Zhang, H. Ming, Z.Y. Wu, A new iterative algorithm to reconstruct the refractive index, Phys. Med. Biol. 52 (2007) L5.
[45] Y. Liu, F. Meirer, P.A. Williams, J. Wang, J.C. Andrews, P. Pianetta, TXM-wizard: a program for advanced data collection and evaluation in full-field transmission X-ray microscopy, J. Synchrotron Radiat. 19 (2012) 281–287.